# Modeling of hydraulic fracture problem in partially saturated porous media using cohesive zone model

**F. Dastjerdy[1], O.R. Barani[2], F. Kalantary[2],***

*Abstract*

*In this paper, a finite element model is developed for the fully hydro-mechanical analysis of hydraulic fracturing in partially saturated porous media. The model is derived from the framework of generalized Biot theory. The fracture propagation is governed by a cohesive fracture model. The flow within the fracture zone is modeled by the lubrication equation. The displacement of solid phase, and the pressure of wetting and non-wetting phases are considered as the main unknown parameters. Other variables are incorporated into the model using empirical relationships between saturation, permeability and capillary pressure. Zero-thickness element and conventional bulk element are used for propagating fracture and the surrounding media, respectively. The model is validated with respect to analytical solution of hydraulic fracture propagation problem in saturated media and then the problem is solved in semi-saturated media, considering the wetting and non-wetting pore fluid.*

*Keywords: Hydraulic fracture, Partially saturated media, Cohesive fracture, Tow-phase fluid flow, Modeling.*

## 1. Introduction

Modeling the hydraulic fractures in a porous medium is an important problem. Because these discontinuities affect the hydro-mechanical properties of porous media, which has practical applications in a broad range of engineering areas. Hydraulic fracturing is a commonly used method in petroleum engineering to enhance reservoir permeability and performance.

Modeling the hydraulic fracture is a challenging problem because it involves several coupled phenomena such as coupling between the flow of wetting and non-wetting phases in pore spaces, exchanging of fluid between the continuum porous media and the induced discontinuity, the deformation of solid phase, and opening or closing of the discontinuity.

Issues related to porous medium have been studied by various researchers; Ghasemzadeh [1] formulated mathematically solute transport with considering heat and water flow in deformable porous media, Luo [2] developed a new piping model in the framework of continuum mixture theory. He assumed that porous media are comprised of solid skeleton phase, fluid phase and fluidized fine particles phase.

Ashayeri et al [3] presented time domain fundamental solutions for the extended Biot's dynamic formulations of two-dimensional (2D) unsaturated poroelasticity. They considered unsaturated porous media as a porous media in which the voids are saturated with two immiscible fluids, i.e. liquid and gas. Attia et al [4] studied the unsteady flow in porous medium of a viscous incompressible fluid bounded by two parallel porous plates with heat transfer.

Problems which deal with fluid flow in a discontinuity and its surrounding porous media have been studied by using different methods; Simoni and Secchi [5] introduced the double-node interface element in saturated porous media, Schrefler et al. [6] and Secchi et al. [7] modeled the hydraulic fracture in saturated porous media with mesh adaption technique, Segura and Carol [8] proposed a model for the saturated porous media using zero-thickness elements to model discontinuity, Rethore et al [9] presented the fluid flow in unsaturated porous media with passive gas phase, taking into account changes in the permeability due to the progressive damage evolution inside the cohesive zone. Adachi and Detournay [10] obtained the semi-analytic asymptotic solutions corresponding to small and large time for hydraulic fracture problems. Chen et al [11] established a finite element model based on the pore pressure cohesive finite elements to investigate the propagation of a penny-shaped hydraulic fracture in an infinite elastic medium, and investigated the effect of cohesive material parameters and fluid viscosity on the hydraulic fracture behavior. Lecampion [12] investigated the extended finite element

* Corresponding author: fz_kalantary@kntu.ac.ir

1 M.Sc. of Geotechnical Engineering, Faculty of Civil Engineering, K.N.Toosi University of Technology
2 Assistant Professor, Geotechnical. Department, Faculty of Civil Engineering, K.N.Toosi University of Technology

method for the solution of hydraulic fracture problems and introduced special tip functions such as encapsulating tip asymptotic, which is typically encountered in hydraulic fractures. Kovalyshen [13] studied the large-scale 3D diffusion around the fracture and its associated poroelastic effects on fracture propagation. Sarris and Papanastasiou [14] studied the importance of the cohesive zone in the modeling of a fluid driven fracture under plain strain conditions. Barani et al. [15] modeled the cohesive crack growth in partially saturated media, and Khoei et al. [16] developed a formulation for double-node interface element in dynamic fracture propagation. Khoei and Haghighat [17] and also Mohamadnejad and Khoei [18] modeled the fluid flow respectively in saturated and partially saturated porous media with weak discontinuity using extended finite element method. Carrier and Granet [19] demonstrated the ability of cohesive zone model in simulating the hydraulic fracture in the four limiting propagation regimes in which toughness-fracture storage, toughness-leak-off, viscosity-fracture storage and viscosity-leak-off dominated. Chen [20] investigated some important issues such as mesh transition and far-field boundary approximation in the cohesive finite element model of the hydraulic fracturing process. Sarris and Papanastasiou [21] investigated the main parameters that influence the propagation of a fluid-driven fracture in a poroelastoplastic continuum. These parameters include the cohesive zone, the stress anisotropy and the pore pressure field. Ru et al [22] investigated the extended finite element method for the solution of the plane strain problem of a hydraulic fracture propagating in an impermeable elastic medium.

In all of the works mentioned above, the gas phase is assumed to be negligible. It should also be stated that Mohamadnejad and Khoei [23] modeled the cohesive crack growth in partially saturated porous media using extended finite element method.

In this paper, a numerical method is described to model the hydro-mechanical progress both of the fracture and porous media in the finite element analysis framework. For this work, a zero-thickness element is developed to model the discontinuity. Fracture propagation is governed by a cohesive law. In order to describe the fracture and partially saturated porous media, momentum and mass balance equation with Darcy law for each fluid phase are employed. The standard Galerkin method and Newmark scheme are used for discretization in space and time respectively. The hydraulic fracture problem in saturated media is solved to confirm accuracy of the present model. Finally, taking gas pressure into account, this problem is evaluated in partially saturated porous media.

## 2. Physical Model

The semi-saturated porous medium is modeled as a mixture of solid skeleton, water (as wetting phase) and gas (as non-wetting phases). The fluid flow through the porous medium is considered immiscible and it is assumed that there is no phase change and no mass transfer between fluid phases.

The water pressure $p_w$ the gas pressure $p_g$ and the displacement of solid skeleton are the main variables and other variables are incorporated in the model using empirical relationship between water saturation, permeability and capillary pressure.

The capillary pressure $p_c$ between two fluid phases is defined as the difference between the water pressure and the gas pressure:

$$P_c = P_g - P_w \tag{1}$$

In partially saturated porous media, the voids of skeleton are filled partly with water and partly with gas and therefore degree of saturation of water $S_w$ and gas $S_g$ always sum to unity:

$$S_w + S_g = 1 \tag{2}$$

In the theory of porous media, modified effective stress is an essential concept for the deformation of solid skeleton:

$$\sigma'' = \sigma + \alpha m p \tag{3}$$

In which $\sigma$ is total stress vector, $\sigma''$ is the modified effective stress vector, $m$ is the identity vector defined as $\begin{bmatrix} 1 & 1 & 0 \end{bmatrix}^T$ for two dimensional case, $p$ is the mean pressure of fluid surrounding the grains, which is given by averaging technique $p = S_w p_w + S_g p_g$ , and $\alpha$ is the Biot constant which depends on the material type and defined as $\alpha = 1 - {K_t}/{K_s} \leq 1$, where $K_t$ and $K_s$ denote the bulk modules of the porous medium and solid particles, respectively.

The constitutive relationship for the solid skeleton is expressed as

$$d\sigma'' = D\,d\varepsilon \tag{4}$$

Where $D$ is tangential constitutive matrix defined by suitable constitutive law. $d\sigma''$ and $d\varepsilon$ are the modified effective stress increment and strain increment, respectively.

## 3. Governing Equation of Multiphase Porous Media

In order to describe the behavior of partially saturated porous media, the linear momentum balance equation and fluids mass balance equation are used. Neglecting relative acceleration of fluid phases with respect to acceleration term of the solid phase, the linear momentum balance equation for the multiphase porous media can be written as

$$\nabla^T .\sigma + \rho b - \rho \ddot{u} = 0 \tag{5}$$

*F. Dastjerdy, O.R. Barani, F. Kalantary*

Where $\ddot{u}$ is the acceleration vector of solid phase, $b$ is body force per unit mass and $\rho$ indicates the average density of total mixture defined as $\rho = (1-n)\rho_s + n(S_w\rho_w + S_g\rho_g)$, in which $n$ denotes porosity, $\rho_s, \rho_w$ and $\rho_g$ are the densities of the solid phase, water and gas fluid phases, respectively, and $\nabla$ denotes del operator.

The mass balance equation for each fluid phase is combined with the general form of Darcy's law to describe the flow behavior of the porous medium under the influence of solid skeleton deformation [24].

$$
\begin{aligned}
&(\frac{\alpha-n}{K_s}S_w^2 + \frac{nS_w}{K_w})\frac{\partial p_w}{\partial t} + \frac{\alpha-n}{K_s}S_wS_g\frac{\partial p_g}{\partial t} + \alpha S_w m^T L\frac{\partial u}{\partial t} \\
&+(\frac{\alpha-n}{K_s}S_wp_w - \frac{\alpha-n}{K_s}S_wp_g + n)\frac{\partial S_w}{\partial t} + \nabla^T[\frac{Kk_{rw}}{\mu_w}(-\nabla p_w + \rho_w(b-\ddot{u}))] = 0 \\
&(\frac{\alpha-n}{K_s}S_g^2 + \frac{nS_g}{K_g})\frac{\partial p_g}{\partial t} + \frac{\alpha-n}{K_s}S_gS_w\frac{\partial p_w}{\partial t} + \alpha S_g m^T L\frac{\partial u}{\partial t} \\
&+(\frac{\alpha-n}{K_s}S_gp_g - \frac{\alpha-n}{K_s}S_wp_g + n)\frac{\partial S_g}{\partial t} + \nabla^T[\frac{Kk_{rg}}{\mu_g}(-\nabla p_g + \rho_g(b-\ddot{u}))] = 0
\end{aligned}
\tag{6}
$$

where $K_s, K_w$ and $K_g$ are the bulk modulus of solid phase, water and gas fluid phases, respectively.

$K$ denotes the intrinsic permeability which is assumed to be isotropic, $k_{rw}, k_{rg}$ are the relative permeability of water and gas fluid phases which depends on the degree of saturation through suitable experimental function and $\mu_w, \mu_g$ denote the dynamic viscosity of water and gas phases, respectively, the differential operator $L$ is defined as:

$$
L^T = \begin{bmatrix}
\partial/\partial x & 0 & 0 & \partial/\partial y & 0 & \partial/\partial z \\
0 & \partial/\partial y & 0 & \partial/\partial x & \partial/\partial z & 0 \\
0 & 0 & \partial/\partial z & 0 & \partial/\partial y & \partial/\partial x
\end{bmatrix}
$$

Derivative of the saturation degree with respect to the time is expressed as follows:

$$
\begin{aligned}
&n\frac{\partial S_w}{\partial t} = n\frac{\partial S_w}{\partial P_c}\frac{\partial P_c}{\partial t} = C_s(\frac{\partial P_g}{\partial t} - \frac{\partial P_w}{\partial t}) \\
&C_s = n\frac{\partial S_w}{\partial P_c}
\end{aligned}
\tag{7}
$$

Numerical solution of a field problem requires the knowledge of the corresponding value of the field variable associated with the initial and boundary conditions (Fig. 1). The initial boundary value of displacement and pressure field are specified as follows:

$$
\begin{aligned}
u &= u^0 \quad on \quad \Gamma_u \\
p_w &= p^0_w \quad on \quad \Gamma_{p_w} \qquad at \quad t=0 \\
p_g &= p^0_g \quad on \quad \Gamma_{p_g}
\end{aligned}
\tag{8}
$$

Which are in general obtained by means of a preliminary static solution to guarantee the satisfaction of the governing equation at t=0. In relation (8), $\Gamma_u$, $\Gamma_{p_w}$ and $\Gamma_{p_g}$ are parts of external boundary with prescribed displacement, water pressure and gas pressure, respectively.
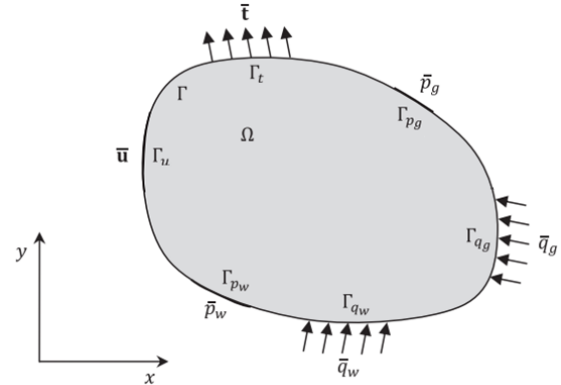


**Fig. 1** Boundary conditions of the body $\Omega$

The natural boundary condition is imposed on the boundary as prescribed traction or external displacement for the displacement field as:

$$
u_i = \hat{u}_i \quad on \quad \Gamma_u; \quad \sigma_{ij}n_i = t_j \quad on \quad \Gamma_t
\tag{9}
$$

where $\Gamma_t$ is a part of external boundary with specified traction and $t_j$ is the prescribed traction applied on the boundary $\Gamma_t$, and $n_i$ is the unit outward normal vector to the external boundary $\Gamma_t$, and $\Gamma = \Gamma_u \cup \Gamma_t$

The boundary condition for water and gas pressure field are as:

$$
\begin{aligned}
&for \; gas \; pressure \\
&p_g = \hat{p}_g \; on \; \Gamma_{p_g}; \\
&\rho_g\frac{K}{\mu^g}(-\text{grad}p_g + \rho_g(b-\ddot{u}))^T.n = q_g \; on \; \Gamma_{q_g}; \\
&for \; water \; pressure \\
&p_w = \hat{p}_w \; on \; \Gamma_{p_w}; \\
&\rho_w\frac{K}{\mu_w}(-\text{grad}p_w + \rho_w(b-\ddot{u}))^T.n = q_w \; on \; \Gamma_{q_w};
\end{aligned}
\tag{10}
$$

where $\Gamma_{q_g}$ and $\Gamma_{q_g}$ are parts of external boundary with specified gas and water normal outflow, respectively. $q_g$ and $q_w$ are the prescribed outflow rates of the porous fluid imposed on permeable boundaries $\Gamma_{q_g}$ and $\Gamma_{q_w}$, respectively, and $\Gamma = \Gamma_{p_w} \cup \Gamma_{q_w} = \Gamma_{p_g} \cup \Gamma_{q_g}$.

For numerical solution, Eqs. (5)-(6) are discretized in space by finite Galerkin method and in time by Newmark scheme. The unknown variables are expressed in terms of their nodal values by means of global shape functions as:

$$
u = N^u\bar{u}; \; p_w = N^p\bar{p}_w; \; p_g = N^p\bar{p}_g
\tag{11}
$$

Based on the standard Galerkin technique Eqs.(5)-(6) are transferred into a set of matrix form as:

$$M\ddot{u} + \int_\Omega B^T \sigma d\Omega - C_{sw}\bar{p}_w - C_{sg}\bar{p}_g = f_u$$

$$C_{sw}{}^T \frac{\partial \bar{u}}{\partial t} + P_{ww}\frac{\partial \bar{P}_w}{\partial t} + C_{wg}\frac{\partial \bar{P}_g}{\partial t} + H_{ww}\bar{P}_w = f_w \tag{12}$$

$$C_{sg}{}^T \frac{\partial \bar{u}}{\partial t} + C_{gw}\frac{\partial \bar{P}_w}{\partial t} + P_{gg}\frac{\partial \bar{P}_g}{\partial t} + H_{gg}\bar{P}_g = f_g$$

Where B is the strain-displacement matrix. The definition of all the coefficient matrices and the load and flow vectors are listed in Appendix A.

The Newmark scheme adopted for time integration, the first and second order time derivates of the variable are written as a function of the solution at previous step and their current increment,

$$\ddot{u}^{n+1} = a_0(u^{n+1} - u^n) - a_2\dot{u}^n - a_3\ddot{u}^n,$$
$$\dot{u}^{n+1} = a_1(u^{n+1} - u^n) - a_4\dot{u}^n - a_5\ddot{u}^n, \qquad \pi = w, g$$
$$\ddot{p}_\pi{}^{n+1} = a_0(p_\pi{}^{n+1} - p_\pi{}^n) - a_2\dot{p}_\pi{}^n - a_3\ddot{p}_\pi{}^n, \tag{13}$$
$$\dot{p}_\pi{}^{n+1} = a_1(p_\pi{}^{n+1} - p_\pi{}^n) - a_4\dot{p}_\pi{}^n - a_5\ddot{p}_\pi{}^n,$$

where in above equations:

$$a_0 = \frac{1}{\beta.\Delta t^2}, \; a_1 = \frac{\delta}{\beta.\Delta t}, \; a_2 = \frac{1}{\beta.\Delta t}, \; a_3 = \frac{1}{2\beta} - 1, \; a_4 = \frac{\delta}{\beta} - 1, \; a_5 = \Delta t(\frac{\delta}{2\beta} - 1)$$

$\Delta t$ is time increment; furthermore, $\beta$ and $\delta$ are the Newmark parameters. To guarantee the unconditional stability of the time integration procedure, the Newmark parameter must be chosen as $\beta \geq 0.25(0.5 + \delta)^2$, $\delta \geq 0.5$.

## 4. Formulation of Cohesive Fracture Zone

The main concept of cohesive zone is based on the fact that in the cohesive zone, called fictitious process zone (FPZ), the stress can be transferred through the fictitious crack sides. In this model, if the crack tip stress reaches the tensile strength of material, the fictitious crack grows. By opening the crack, the crack surface does not become stress free, but its stress decreases by increasing the crack width according to a cohesive law. Various traction-separation laws have been used by researchers in the modeling of cohesive material. In this study, a bilinear cohesive law, which was originally proposed by Espinosa and Zavattier [25] is used. The fracturing material in the zone of fractured media undergoes the mixed mode crack opening, in which the crack moves along an interface separating two solid openings. In this model, the effective traction and effective displacement are resolved into normal and tangential component as:

$$t_e = \sqrt{t_n^2 + t_s^2}$$
$$\delta_e = \sqrt{\delta_n^2 + \delta_s^2} \tag{14}$$

where $t_e$ is the effective traction, $t_n$ and $t_s$ are the

normal and shear traction, respectively; $\delta_e$ is the effective displacement; furthermore, $\delta_n$ and $\delta_s$ are the normal displacement and shear sliding of fracture surfaces. The non-dimensional effective displacement is defined as [26]:

$$\lambda_e = \sqrt{\left(\frac{\delta_n}{\delta_c}\right)^2 + \left(\frac{\delta_s}{\delta_c}\right)^2} \tag{15}$$

where $\delta_c$ denotes the critical displacement that is proportional to complete separation, i.e. zero traction.

Fig. 2 shows the bilinear cohesive law in terms of normalized opening tractions and normalized opening displacement. The pre-peak region represents the elastic part of the intrinsic cohesive law, whereas the softening portion after the peak load accounts for the damage occurring in the fracturing process zone. The parameter $\lambda_{cr}$ is a dimensionless displacement which corresponds to the maximum traction and is set to a small value to obtain more exact result. The normal and shear tractions can be obtained as:

$$t_n = \frac{\sigma_c}{\lambda_{cr}}\left(\frac{\delta_n}{\delta_c}\right) \qquad \text{if } \lambda_e < \lambda_{cr}$$

$$t_n = \frac{\sigma_c}{\lambda_e}\frac{1 - \lambda_e}{1 - \lambda_{cr}}\left(\frac{\delta_n}{\delta_c}\right) \qquad \text{if } \lambda_e > \lambda_{cr} \text{ (loading)} \tag{16}$$

$$t_n = \frac{\sigma_c}{\lambda_{e1}}\frac{1 - \lambda_{e1}}{1 - \lambda_{cr}}\left(\frac{\delta_n}{\delta_c}\right) \qquad \text{if } \lambda_e > \lambda_{cr} \text{ (unloading)}$$

$$t_s = \frac{\sigma_c}{\lambda_{cr}}\left(\frac{\delta_s}{\delta_c}\right) \qquad \text{if } \lambda_e < \lambda_{cr}$$

$$t_s = \frac{\sigma_c}{\lambda_e}\frac{1 - \lambda_e}{1 - \lambda_{cr}}\left(\frac{\delta_s}{\delta_c}\right) \qquad \text{if } \lambda_e > \lambda_{cr} \text{ (loading)} \tag{17}$$

$$t_s = \frac{\sigma_c}{\lambda_{e1}}\frac{1 - \lambda_{e1}}{1 - \lambda_{cr}}\left(\frac{\delta_s}{\delta_c}\right) \qquad \text{if } \lambda_e > \lambda_{cr} \text{ (unloading)}$$
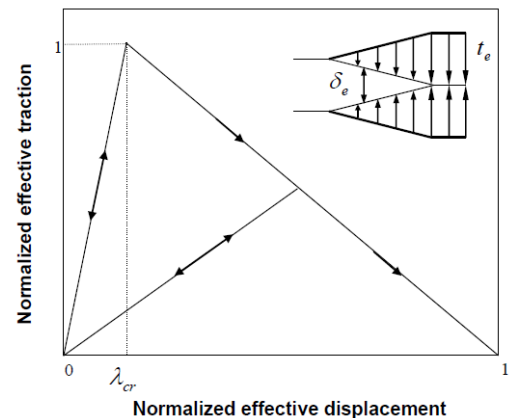


**Fig. 2** a bilinear cohesive law in the term of normalized effective displacement and normalized effective traction

where $\sigma_c$ is the material strength and $\lambda_{e1}$ is the non-dimensional displacement just before unloading. The value of critical displacement is usually computed by the

*F. Dastjerdy, O.R. Barani, F. Kalantary*

cohesive fracture energy $G_c$ assumed as a material property and computed by equating the area under the displacement-traction curve, namely $G_c = \frac{1}{2}\delta_c\sigma_c$.

In order to derive the components of cohesive material matrix $C_f$ for the fracture zone, it is required to differentiate traction with respect to normal and shear displacements [26]. Hence, the components of cohesive material matrix $C_f$ for $\lambda_e < \lambda_{cr}$ are governed by

$$\mathbf{C}_f = \begin{bmatrix} C_{ss} & C_{sn} \\ C_{ns} & C_{nn} \end{bmatrix} = \begin{bmatrix} \dfrac{\partial t_s}{\partial \delta_s} & \dfrac{\partial t_s}{\partial \delta_n} \\ \dfrac{\partial t_n}{\partial \delta_s} & \dfrac{\partial t_n}{\partial \delta_n} \end{bmatrix} = \begin{bmatrix} \dfrac{\sigma_c}{\lambda_{cr}\delta_c} & 0 \\ 0 & \dfrac{\sigma_c}{\lambda_{cr}\delta_c} \end{bmatrix} \tag{18}$$

If $\lambda_e > \lambda_{cr}$, the components of $C_f$ matrix in the case of loading are given by

$$\mathbf{C}_f = \begin{bmatrix} C_{ss} & C_{sn} \\ C_{ns} & C_{nn} \end{bmatrix} = \begin{bmatrix} \dfrac{\partial t_s}{\partial \delta_s} & \dfrac{\partial t_s}{\partial \delta_n} \\ \dfrac{\partial t_n}{\partial \delta_s} & \dfrac{\partial t_n}{\partial \delta_n} \end{bmatrix}$$

$$= \begin{bmatrix} -\dfrac{\delta_c\sigma_c}{1-\lambda_{cr}}\left(\dfrac{\delta_s}{\lambda_e\delta_c^2}\right)^2 + (1-\lambda_e)\dfrac{\delta_c\sigma_c}{1-\lambda_{cr}}\left(\dfrac{1}{\lambda_e\delta_c^2} - \dfrac{1}{\lambda_e^3}\dfrac{\delta_s^2}{\delta_c^4}\right) \\ -\dfrac{\delta_c\sigma_c}{1-\lambda_{cr}}\dfrac{1}{\lambda_e^3}\left(\dfrac{\delta_s}{\delta_c^2}\right)\left(\dfrac{\delta_n}{\delta_c^2}\right) \end{bmatrix}$$
$$\left. \begin{array}{c} -\dfrac{\delta_c\sigma_c}{1-\lambda_{cr}}\dfrac{1}{\lambda_e^3}\left(\dfrac{\delta_s}{\delta_c^2}\right)\left(\dfrac{\delta_n}{\delta_c^2}\right) \\ -\dfrac{\delta_c\sigma_c}{1-\lambda_{cr}}\left(\dfrac{\delta_n}{\lambda_e\delta_c^2}\right)^2 + (1-\lambda_e)\dfrac{\delta_c\sigma_c}{1-\lambda_{cr}}\left(\dfrac{1}{\lambda_e\delta_c^2} - \dfrac{1}{\lambda_e^3}\dfrac{\delta_n^2}{\delta_c^4}\right) \end{array} \right] \tag{19}$$

And in the case of unloading, they are given by

$$\mathbf{C}_f = \begin{bmatrix} C_{ss} & C_{sn} \\ C_{ns} & C_{nn} \end{bmatrix} = \begin{bmatrix} \dfrac{\partial t_s}{\partial \delta_s} & \dfrac{\partial t_s}{\partial \delta_n} \\ \dfrac{\partial t_n}{\partial \delta_s} & \dfrac{\partial t_n}{\partial \delta_n} \end{bmatrix}$$
$$= \begin{bmatrix} \dfrac{\sigma_c}{\delta_c}\left(\dfrac{1-\lambda_{e1}}{1-\lambda_{cr}}\right)\dfrac{1}{\lambda_{e1}} & 0 \\ 0 & \dfrac{\sigma_c}{\delta_c}\left(\dfrac{1-\lambda_{e1}}{1-\lambda_{cr}}\right)\dfrac{1}{\lambda_{e1}} \end{bmatrix} \tag{20}$$

## 5. FE Formulation of Fractured Media

In order to perform the finite element model for fracture media, equilibrium equation are implemented similar to section0. The momentum balance of fractured media can be written according to the cohesive fracture behavior similar to Eq.(5) as:

$$\nabla^T.\sigma + \rho b - \rho\ddot{u} = 0 \tag{21}$$

The balance of fluid mass for the fractured media can be rewritten according to Eq.(6) as:

$$\frac{\partial}{\partial l}\left(-k_{r\pi}(k_f)_{sn}\left(\frac{\partial p_m}{\partial l} + \rho_w(\ddot{u}-b)\frac{\partial z_m}{\partial l}\right)\right) + \tag{22}$$
$$\frac{1}{w}\frac{\partial w}{\partial t} + \frac{nS_\pi}{K_\pi}\frac{dp_m}{dt} + \frac{\partial S_\pi}{\partial t} = 0$$
$$i,j = s,n, \quad \pi = w,g$$

where $w$ is the fracture aperture, $k_{r\pi}$ is the relative permeability of each fluid phase and $(k_f)_{sn}$ is the fracture permeability tensor defined as $k_f = \begin{bmatrix} k_s & 0 \\ 0 & k_n \end{bmatrix}$ in which $k_s$ and $k_n$ are the longitudinal and transvers permeability coefficients, respectively.

Eqs. (21)-(22) are discretized in space by using a Galerkin method as:

$$M\ddot{\bar{u}} + K_T\bar{u} - C_{sw}\bar{p}_w - C_{sg}\bar{p}_g = f_u$$
$$C_{sw}{}^T\frac{\partial\bar{u}}{\partial t} + P_{ww}\frac{\partial\bar{P}_w}{\partial t} + C_{sg}\frac{\partial\bar{P}_g}{\partial t} + H_{ww}\bar{P}_w = f_w \tag{23}$$
$$C_{sg}{}^T\frac{\partial\bar{u}}{\partial t} + C_{gw}\frac{\partial\bar{P}_w}{\partial t} + P_{gg}\frac{\partial\bar{P}_g}{\partial t} + H_{gg}\bar{P}_g = f_g$$

where the cohesive stiffness matrix $K_T$ is defined as $\int_\Omega B_f^T D_f B_f^T d\Omega$, in which $D_f = wC_f$, with the cohesive material matrix $C_f$ is defined in Eqs.(18-20). Calculation of $K_T$ has been given in detail in [26] other matrices are listed in Appendix B.

## 6. Numerical Simulation Results

In order to demonstrate a part of the wide range of problems that can be solved by the present approach and to illustrate the performance of the computational algorithm in the modeling of partially saturated porous media problem, the hydraulically driven fracture propagation problem is solved. First, in order to verify the accuracy of the finite element solution, this problem is presented against an analytical solution assuming saturated condition, and then it is solved in partially saturated condition.

### 6.1. Hydraulic fracture modeling in statured media

To evaluate the accuracy of the finite element solution of crack growth in statured porous media a horizontal section plane strain model is considered. An analytical solution for this problem was obtained by Spence and Sharp [27] and Geertsma and Klerk [28] and used here for comparison. A numerical solution for this example was carried out by Boone and Ingraffea [29], in which a finite element method was applied for the mechanical problem and a finite difference method was used for flow analysis through the fracture In Fig. 3 the geometry, boundary condition and finite element mesh and the material properties are presented in Table 1.Triangular elements with linear interpolation functions are used. An initial

crack is assumed at the borehole and constant flow rate of $0.0001^{m^3}/_s$ is imposed at the crack mouth which causes the initial crack propagation. The tensile strength of the material is assumed 0.5MPa. When the maximum effective stress at the crack tip reaches the tensile strength of the material, a new node is inserted at the crack tip and the mesh is modified accordingly so that the crack propagates perpendicular to the maximum effective stress.
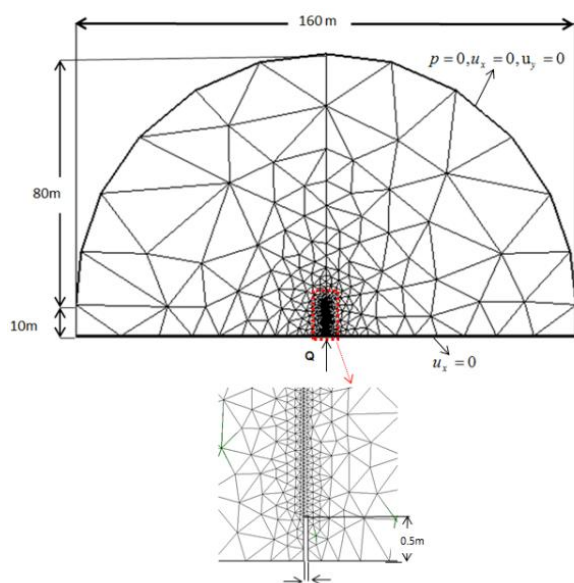


**Fig. 3** the geometry and boundary condition of hydraulic fracture problem

In Fig. 4 the variation of crack mouth pressure with time is plotted and it is compared with analytical solution [27,28]. As can be seen from this figure, the present simulation result is in good agreement with analytical solution. Fig. 5 shows the contour of maximum effective stress at 1.0, 4.0, 7.0 and 10 s. In Fig. 6 the water pressure at t=5 and 10 s are presented.

**Table 1** material properties for hydraulic fracturing problem

| Elasticity modulus | $E = 15.96\,MPa$ |
|---|---|
| Biot coefficient | $\alpha = 0.79$ |
| Poisson's ratio | $v = 0.2$ |
| porosity | $n = 0.19$ |
| Solid phase density | $\rho_s = 2000\,{}^{kg}/_{m^3}$ |
| Water density | $\rho_w = 1000\,{}^{kg}/_{m^3}$ |
| Gas density | $\rho_g = 1.2\,{}^{kg}/_{m^3}$ |
| Bulk modulus of solid phase | $K_s = 36\,GPa$ |
| Bulk modulus of water | $K_w = 3\,GPa$ |
| Bulk modulus of gas | $K_g = 0.1\,MPa$ |
| Intrinsic permeability | $k = 6\times10^{-15}\,m^2$ |
| Dynamic viscosity of water | $\mu_w = 0.1\times10^{-3}\,Pa\,s$ |
| Dynamic viscosity of gas | $\mu_g = 1.8\times10^{-5}\,Pa\,s$ |
| Atmospheric pressure | $p_{atm} = 0\,kPa$ |
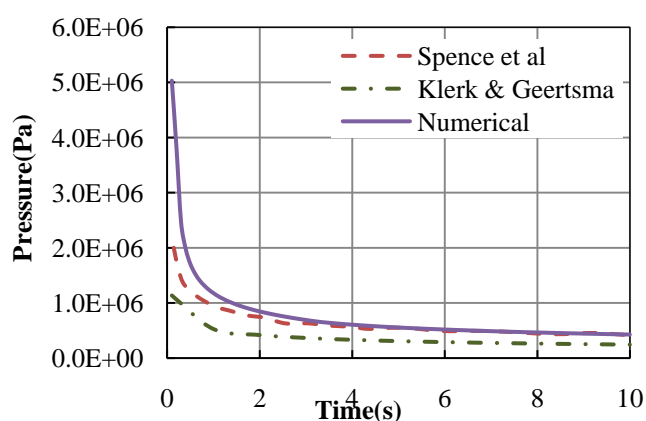


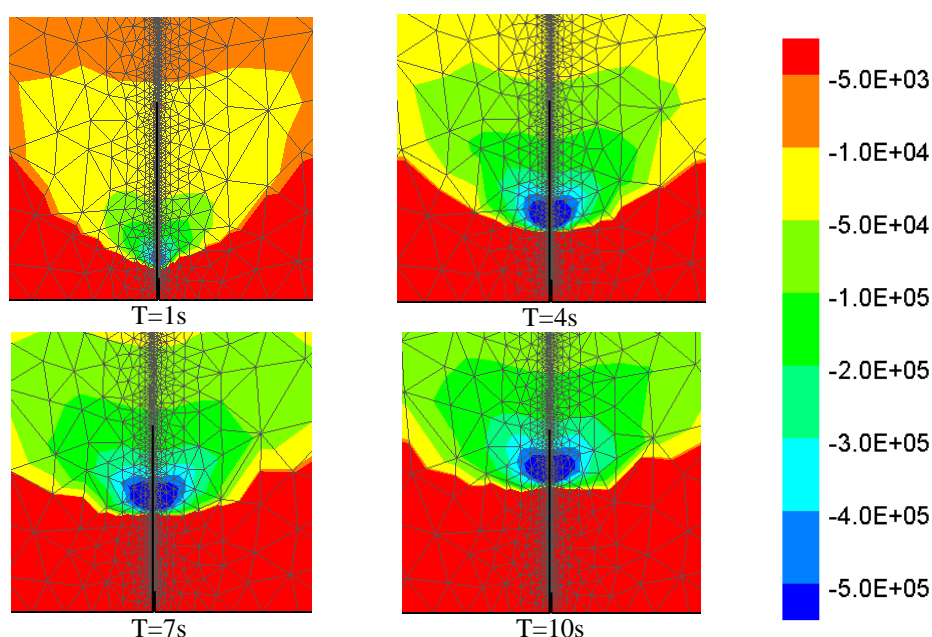**Fig. 4** the variation of crack mouth pressure with time and compare with analytical solution [28,29]



T=1s    T=4s

T=7s    T=10s

**Fig. 5** contour of maximum effective stress in various time steps (all dimensions in Pa)

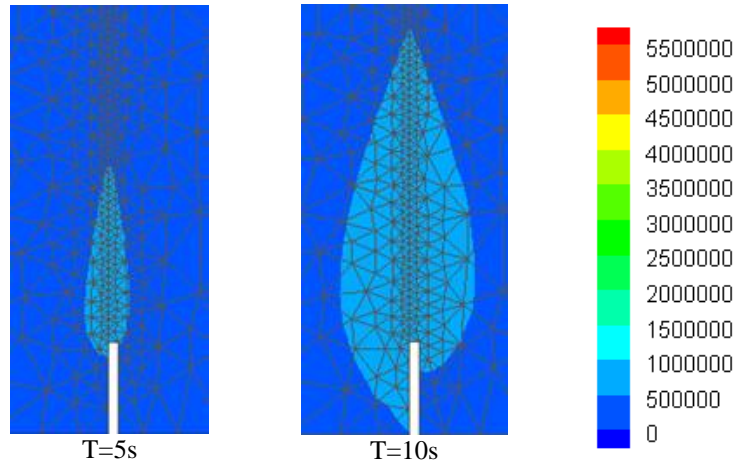*F. Dastjerdy, O.R. Barani, F. Kalantary*

T=5s　　　　　T=10s

**Fig. 6** contour of water pressure at various time steps (all dimensions in Pa)

*6.2. Hydraulic fracture modeling in partially statured porous media*

In this section, the hydraulic fracture example is considered in unsaturated condition. The initial saturation is assumed 0.93, which is proportional with initial water pressure -100000Pa and initial gas pressure -10 Pa. In this example, the following water saturation-capillary pressure relation given by Brooks [30] has been used:

$$S_w = 1 - (\frac{P_c}{-40 \times 9.81 \times 980})^2 \tag{24}$$

The relation between water saturation-relative permeability is defined by VanGenuchten [31] as

$$S_{eff} = \frac{S_w - S_{rw}}{1 - S_{rw}}$$

$$K_{rg} = S_{eff}^{\frac{3+3\lambda}{3}} \tag{25}$$

$$K_{rw} = (1 - S_{eff})^2 (1 - S_{eff}^{\frac{2+\lambda}{\lambda}})$$

where the residual water saturation $S_{rw} = 0.2$, the pore size distribution index $\lambda = 3$ and $S_{eff}$ denote the effective water saturation.

Fig. 7 shows the variation of crack mouth water pressure with time. In Fig. 8 and 9 the results of water pressure and saturation are presented at t=25, 50 and 200s. Fig. 10 shows the contour of gas pressure at t=25, 50 and 200s. As shown in this figure, a significant gas pressure develops during hydraulic fracturing process in the unsaturated media.
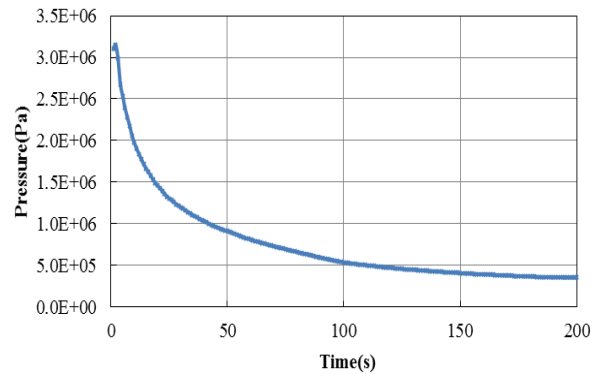


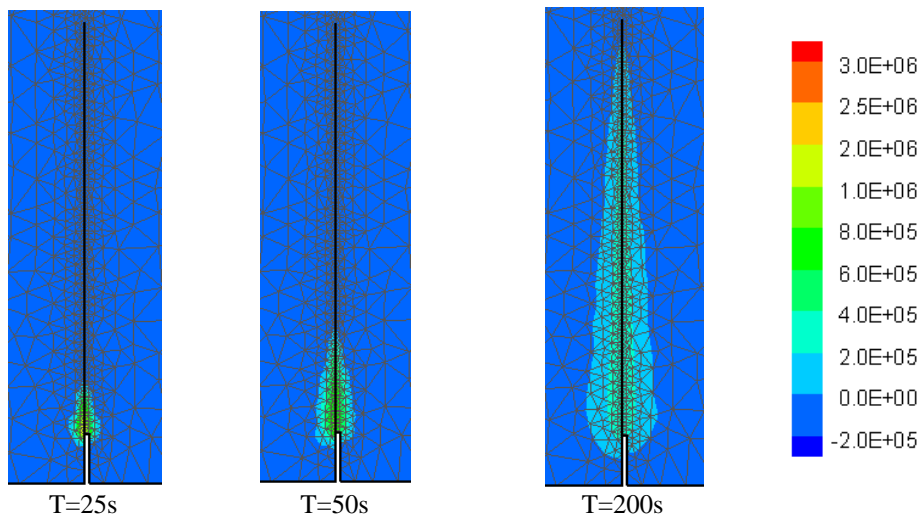**Fig. 7** variation of crack mouth water pressure with time



T=25s　　　　　T=50s　　　　　T=200s

**Fig. 8** contour of water pressure at various time steps (all dimensions in Pa)
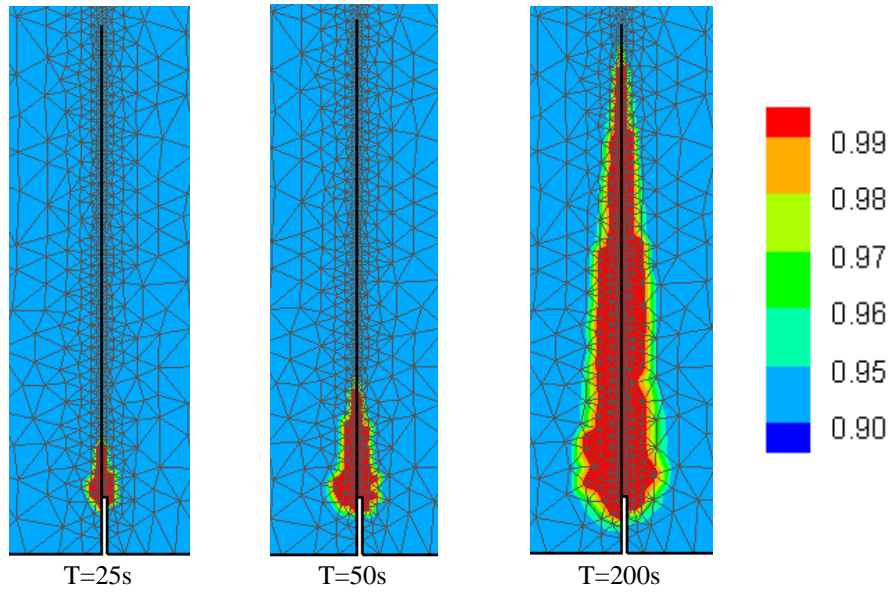
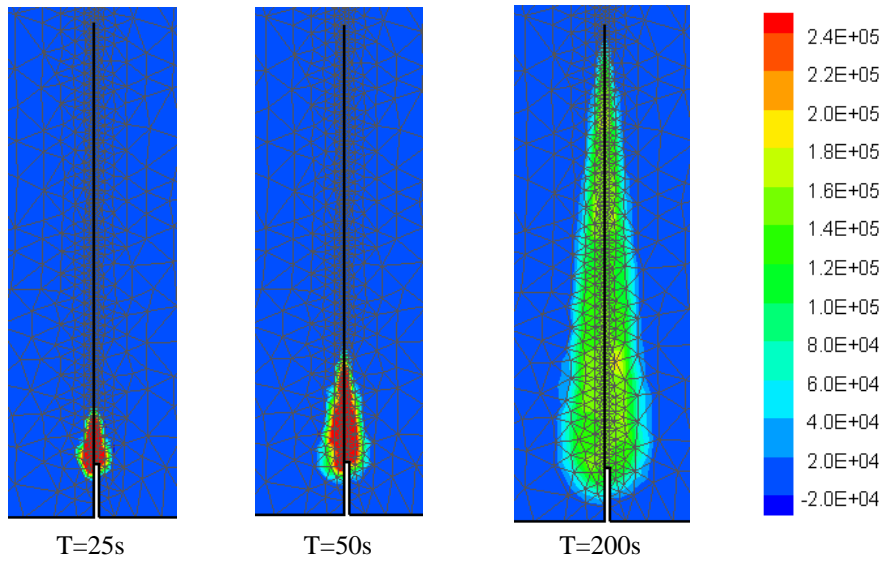**Fig. 9** contour of water saturation at various time steps



**Fig. 10** contour of gas pressure at various time steps (all dimensions in Pa)

## 7. Conclusion

In this paper, a finite element model has been developed for numerical solution of cohesive fracture in partially saturated porous media, considering two phase flow. In order to describe the behavior of multiphase porous media the governing equation including momentum balance equation and fluid mass balance equation was applied for each fluid phase. A spatial discretization by means of Galerkin method in term of solid displacement, water and gas pressure and a time discretization by general Newmark method have been used to yield the final system of equation. The double nodded zero-thickness cohesive interface element was employed to present fracture behavior. The governing equations were rewritten for fracture media to describe the hydro-mechanical behavior of the fracturing multiphase media.

In order to demonstrate the capability of proposed computational algorithm, hydraulic fracture problem was analyzed. The hydraulically driven fracture propagation in saturated condition was solved to verify the algorithm. The example it has been solved with initial saturation 0.93, and the water pressure, gas pressure and water saturation contour for various time steps have been presented. A significant amount for gas pressure was obtained in unsaturated media, as a result of a complete analysis of the hydraulic fracture problem.

## Appendix A

The coefficient matrices in the set of discretized governing equation (12) are defined as follows:

$$\mathbf{f}^u = \int_\Omega (\mathbf{N}^u)^\mathbf{T} \rho b d\Omega + \int_{\Gamma_t} (\mathbf{N}^u)^\mathbf{T} \bar{t} d\Gamma$$

$$M = \int_\Omega (\mathbf{N}^u)^\mathbf{T} \rho N^u d\Omega$$

$$C_{sw} = \int_\Omega B^\mathbf{T} S_w \alpha m N^p d\Omega$$

*F. Dastjerdy, O.R. Barani, F. Kalantary*

$$C_{sg} = \int_\Omega B^{\mathbf{T}} S_g \alpha m N^{\,p} d\Omega$$

$$P_{ww} = \int_\Omega N_p^T \left[ \frac{\alpha-n}{K_s} S_w (S_w - P_w \frac{C_s}{n} + P_g \frac{C_s}{n}) + \frac{nS_w}{K_w} - C_s \right] N_p d\Omega$$

$$C_{wg} = \int_\Omega N_p^T \left[ \frac{\alpha-n}{K_s} S_w (S_g + P_w \frac{C_s}{n} - P_g \frac{C_s}{n}) + C_s \right] N_p d\Omega$$

$$H_{ww} = H = \int_\Omega (\nabla N_p)^T \frac{Kk_{rw}}{\mu_w} \nabla N_p d\Omega$$

$$f_w = \int_\Omega (\nabla N_p)^T \frac{Kk_{rw}}{\mu_w} \rho_w g d\Omega - \int_{\Gamma_w^q} N_p^T \frac{q_w}{\rho_w} d\Gamma$$

$$P_{gg} = \int_\Omega N_p^T \left[ \frac{\alpha-n}{K_s} S_g (S_g - P_g \frac{C_s}{n} + P_w \frac{C_s}{n}) + \frac{nS_g}{K_g} - C_s \right] N_p d\Omega$$

$$H_{gg} = \int_\Omega (\nabla N_p)^T \frac{Kk_{rg}}{\mu_g} \nabla N_p d\Omega$$

$$f_g = \int_\Omega (\nabla N_p)^T \frac{Kk_{rg}}{\mu_g} \rho_g g d\Omega - \int_{\Gamma_g^q} N_p^T \frac{q_g}{\rho_g} d\Gamma$$

## Appendix B

The coefficient matrices in the set of discretized governing equation (23) are defined as follows:

$$f_u = \int_\Omega (N_f^{\,u})^T \rho b d\Omega + \int_{\Gamma_t} (N_f^{\,u})^T \bar{t} d\Gamma$$

$$M = \int_\Omega (N_f^{\,u})^{\mathbf{T}} \rho N_f^{\,u} d\Omega$$

$$C_{sw} = \int_\Omega B_f^{\mathbf{T}} S_w \alpha m N_f^{\,p} d\Omega$$

$$C_{sg} = \int_\Omega B_f^{\mathbf{T}} S_g \alpha m N_f^{\,p} d\Omega$$

$$P_{ww} = \int_\Omega N_f^T \left[ \frac{nS_w}{K_w} - C_s \right] N_f d\Omega$$

$$C_{wg} = \int_\Omega N_f^T C_s N_f d\Omega$$

$$H_{ww} = H = \int_\Omega (\nabla N_f)^T \frac{Kk_{rw}}{\mu_w} \nabla N_f d\Omega$$

$$f_w = \int_\Omega (\nabla N_f)^T \frac{Kk_{rw}}{\mu_w} \rho_w g d\Omega - \int_{\Gamma_w^q} N_f^T \frac{q_w}{\rho_w} d\Gamma$$

$$P_{gg} = \int_\Omega N_f^T \left[ \frac{nS_g}{K_g} - C_s \right] N_f d\Omega$$

$$H_{gg} = \int_\Omega (\nabla N_f)^T \frac{Kk_{rg}}{\mu_g} \nabla N_f d\Omega$$

$$f_g = \int_\Omega (\nabla N_f)^T \frac{Kk_{rg}}{\mu_g} \rho_g g d\Omega - \int_{\Gamma_g^q} N_f^T \frac{q_g}{\rho_g} d\Gamma$$

## References

[1] Ghasemzadeh H. Heat and contaminant transport in unsaturated soil. International Journal of Civil Engineerng, 2008, No. 2, Vol. 6, pp. 90-107.

[2] Luo YL. A continuum fluid-particle coupled piping model based on solute transport, International Journal of Civil Engineering, Transaction B: Geotechnical Engineering, 2013, No. 1, Vol. 11, pp. 38-44.

[3] Ashayeri I, Kamalian M, Jafari MK, Biglari M. Mirmohammad Sadeghi M. Two-dimensional time domain fundamental solution to dynamic unsaturated poroelasticity, International Journal of Civil Engineering, Transaction B: Geotechnical Engineering, 2014, No. 2, Vol. 12, pp. 110-133.

[4] Attia HA, El-Meged WA, Abbas W, Abdeen MAM. Unsteady flow in a porous medium between parallel plates in the presence of uniform suction and injection with heat transfer, International Journal of Civil Engineering, Transaction A: Civil Engineering, 2014, No. 3, Vol. 12, pp. 277-281.

[5] Simoni L, Secchi S. Cohesive fracture mechanics for a multi-phaseporous medium, Engineering Computing, 2003, Vol. 20, pp. 675-698.

[6] Schrefler BA, Secchi S, Simoni L. On adaptive refinement techniques in multi-filed problems including cohesive fracture, Computer Methods in Applied Mechanics and Engineering, 2006, Vol. 195, pp. 444-461.

[7] Secchi S, Simoni L, Scherfler BA. Mesh adaptation and transfer schemes for discrete fracture propagation in porous material, International Journal for Numerical and Analytical Methods, 2007, Vol. 31, pp. 331-345.

[8] Segura JM, Carol I. Coupled HM analysis using zero-thickness interface elements with double nodes, Part I, Theoretical model, International Journal for Numerical and Analytical Methods, 2008, Vol. 32, pp. 2083-2101.

[9] Rethore JR. de Borst, Abellan MA. A two-scale model for fluid flow in an unsaturated porous medium with cohesive cracks, Computational Mechanics, 2008, Vol. 42, pp. 227-238.

[10] Adachi J, Detournay E. Plane strain propagation of a hydraulic fracture in a permeable rock, Engineering Fracture Mechanics, 2008, Vol. 75, pp. 4666-4694.

[11] Chen Z, Bunger A, Zhang Z, Jeffrey R. Cohesive zone finite element-based modeling of hydraulic fractures, Acta Mechanica Solida Sinica, 2009, Vol. 22, pp. 443-452.

[12] Lecampion B. An extended finite element method for hydraulic fracture problems, Communications Numerical Methods in Engineering, 2009, Vol. 25, pp. 121-33.

[13] Kovalyshen Y. Fluid-Driven Fracture in Poroelastic Medium, PhD thesis, University of Minnesota, 2010.

[14] Sarris E, Papanastasiou P. The influence of the cohesive process zone in hydraulic fracturing modelling, International Journal of Fracture, 2011, No. 1, Vol. 167, pp. 33-45.

[15] Barani OR, Khoei AR. Modeling of cohesive crack growth in partially saturated porous media; a study on the permeability of cohesive fracture, International Journal of Fracture, 2011, Vol. 167, pp. 15-31.

[16] Khoei AR, Barani OR. Modeling of dynamic cohesive fracture propagation in porous media, International Journal for Numerical and Analytical Methods, 2011, Vol. 35, pp. 1160-1184.

[17] Khoei AR, Haghighat E. Extended finite element modeling of deformable porous media with arbitrary interfaces, Applied Mathematical Modelling, 2011, Vol. 35, pp. 5426-5441.

[18] Khoei AR, Mohamadnejad T. An extended finite element method for fluid flow in partially saturated porous media with weak discontinuities;the convergence analysis of local enrichment strategies, Computational Mechanics, DOI 10.1007/s00466-012-0732-8, 2012.

[19] Carrier B, Granet S () Numerical modeling of hydraulic fracture problem in permeable medium using cohesive zone model, Engineering Fracture Mechanics, 2012, Vol. 79, pp. 312-328.

[20] Chen Z. Finite element modelling of viscosity-dominated hydraulic fractures, Journal of Petroleum Science and Engineering, 2012, Vols. 88-89, pp. 136-144.

[21] Sarris E, Papanastasiou P. Numerical modeling of fluid-driven fractures in cohesive poroelastoplastic continuum, International Journal for Numerical and Analytical Methods, 2013, Vol. 37, pp. 1822-1846.

[22] Ru Z, Zhao H, Wang M. Numerical modeling of hydraulic fracture propagation using extended finite element method, Poromechanics, 2003, pp. 1923-1929.

[23] Mohamadnejad T, Khoei AR. Hydro-mechanical modeling of cohesive crack propagation in multiphase porous media using the extended finite element method, International Journal for Numerical and Analytical Methods, DOI: 10.1002/nag.2079, 2012.

[24] Lewis RW, Schrefler BA. The finite element method in the staticand dynamic deformation and consolidation of porous media, New York, NY, John Wiley, 1998.

[25] Espinosa HD, Zavattieri PD. A grain level model for the study of failure initiation and evolution in polycrystalline brittle materials, Part I: Theory and numerical implementation, Mechanics of Materials, 2003, Vol. 35, pp. 333-364.

[26] Song SH, Paulino GH, Buttlar WG. A bilinear cohesive zone model tailored for fracture of asphalt concrete considering viscoelastic bulk materia, Engineering Fracture Mechanics, 2006, Vol. 73, pp. 2829-2848.

[27] Spence DA, Sharp P. Self-similar solutions for elasto-hydrodynamic cavity flow, Proceedings of the Royal Society of London, A 400, 1985, Vol. 40, pp. 289-313.

[28] Geertsma J, Klerk F. A rapid method of predicting width and extent of hydraulically induced fractures, Journal of Petroleum Technology, 1969, Vol. 21, pp. 1571-1581.

[29] Boone TJ, Ingraffea AR. A numerical procedure for simulation of hydraulically-driven fracture propagation in poroelastic media, International Journal for Numerical and Analytical Methods, 1990, Vol. 14, pp. 27-47.

[30] Brooks RN, Corey AT. Properties of porous media affecting fluid flow, Journal of Irrigation and Drainage Engineering, 1966, Vol. 92, pp. 61-8.

[31] VanGenuchten. A closed-form equation for predicting the hydraulic conductivity of unsaturated soil, Soil Science Society of America Journal, 1980, Vol. 44, pp. 892–898.

*F. Dastjerdy, O.R. Barani, F. Kalantary*